

Low-loss, high-purity, and ultrabroadband all-fiber LP₄₁ mode converter employing a mode-selective photonic lantern [Invited]

Liang Chen (陈亮), Huiyi Guo (郭慧毅), Zekun Shi (史泽昆), Wenzhe Chang (昌文喆), Boyu Chen (陈柏瑜), Zhi Wang (王志), and Yan-ge Liu (刘艳格)*

Institute of Modern Optics, Nankai University, Tianjin Key Laboratory of Micro-scale Optical Information Science and Technology, Tianjin 300350, China

*Corresponding author: ygliu@nankai.edu.cn

Received September 26, 2023 | Accepted October 20, 2023 | Posted Online November 9, 2023

Broadband mode converters are essential devices for space-division and wavelength-division multiplexing systems. There are great challenges in the generation of higher-order modes above the third order with low loss and high mode purity employing all-fiber devices. In this paper, an all-fiber LP₄₁ mode converter is proposed and fabricated by tapering a nine-core single-mode fiber bundle. Experimental results indicate that this all-fiber LP₄₁ mode converter is low-loss, high-purity, and ultrabroadband. The insertion loss is less than 0.4 dB. The purity of odd LP₄₁ at 1310 nm is 95.09%, and the operating bandwidth exceeds 280 nm.

Keywords: photonic lantern; mode converter; space-division multiplexing.

DOI: [10.3788/COL202321.110008](https://doi.org/10.3788/COL202321.110008)

1. Introduction

High-order modes have potential applications in optical communication^[1,2], particle manipulation^[3], and optical fiber sensing^[4]. Methods to generate higher-order modes have been researched for several decades both in spatial^[5,6] and all-fiber systems^[7–10]. Compared with the spatial mode converters, all-fiber devices have the advantages of small volume and good compatibility. All-fiber high-order mode converters can be achieved through long-period fiber gratings (LPFGs)^[7,8], mode selective couplers (MSCs)^[9], and photonic lanterns (PLs)^[10]. A mode converter employing LPFGs can achieve mode conversion up to LP₄₁^[11,12]. The disadvantage of LPFGs is their narrow working bandwidth. Even worse, as the mode order increases, the difficulty of production and additional insertion losses (ILs) also increase. For example, the 90% conversion efficiency bandwidth of the all-fiber fourth-order mode converter, realized by Chang *et al.* by employing an LPFG written by preset twist, is only 33 nm, and the IL of the LPFG is measured to be as large as 2.4 dB^[1]. MSCs usually have a wider operating bandwidth than LPFGs^[13,14]. Cui *et al.* fabricated MSCs for LP₁₁, LP₂₁, and LP₃₁ modes with minimum losses of 2.5, 1.9, and 1.6 dB, respectively, by the side-polishing method^[13]. By optimizing the polishing process and precise control of phase-matching conditions, MSCs with six-mode groups (LP₀₁, LP₁₁, LP₂₁, LP₀₂, LP₁₂, and LP₃₁) exhibit losses below 1.8 dB, and purity higher than 88.0% in the 1530–1600 nm wavelength range has been achieved

by Zhang *et al.*^[9]. Recently, ultralow-loss five-LP (LP₀₁, LP₁₁, LP₂₁, LP₀₂, and LP₁₂) MSCs with a minimum IL of 0.02 dB (for LP₁₁ mode) and a maximum 90% conversion bandwidth exceeding 174.31 nm (for LP₂₁ mode) were achieved by Guo *et al.* by use of the fused biconical taper method^[14]. However, for the conversion of higher-order modes, the MSCs face an adiabatic transmission dilemma and high cross talk caused by the small difference in effective mode refractive index among high-order modes. Moreover, the precision taper control of large differences in core size between the two optical fibers for higher-order MSCs is also a great challenge.

The mode-group or mode-selective PL is a passive all-fiber device with the characteristics of ultralow loss, large bandwidth, and high capacity, playing the role of mode conversion and mode multiplexing/demultiplexing at the same time. Eznaveh *et al.* experimentally realized the mode selective excitation of LP_{11a}, LP_{11b}, LP_{21a}, and LP_{21b} through a five-core PL, of which the IL was less than 3 dB^[10]. However, when the angular order is higher, modes with different radial orders will degenerate into one mode group due to the close propagation constants. It is difficult to achieve selective excitation of a single high-order mode. For example, Velázquez-Benítez *et al.* experimentally fabricated the 15-core PL multiplexing five LP mode groups, including radial high-order modes through microstructured templates^[15]. LP₃₁ and LP₁₂ degenerated into one mode group, and LP₄₁, LP₂₂, and LP₀₃ degenerated into another mode group. The IL of the

mode group including LP_{41} , LP_{22} , and LP_{03} is also as large as 1–2 dB.

Here, we propose and fabricate a fluorine-doped-fiber-assisted low-loss, high-purity, and ultrabroadband all-fiber LP_{41} mode converter. Selective excitation of LP_{41}^{even} and LP_{41}^{odd} is achieved by tapering a nine-core single-mode fiber bundle with an outer low refractive index capillary. The fluorine-doped fiber at the center of the fiber bundle is used to confine radial high-order modes at the few-mode end of the PL. The operating wavelength of the all-fiber LP_{41} mode converter is measured to cover 1260–1360 nm and 1460–1640 nm using a tunable laser source with limited spectral range. Through numerical mode decomposition of the collected intensity distribution, the purity of LP_{41}^{odd} at 1310 and 1565 nm is estimated to be about 95.09% and 93.37%, respectively. The IL of LP_{41}^{odd} is less than 0.2 dB at 1260–1360 nm and 1460–1640 nm. And the IL of LP_{41}^{even} is less than 0.4 dB at 1260–1360 nm and 1460–1640 nm.

2. Principle

The schematic of the proposed PL is shown in Fig. 1(a). A cross section of the single-mode end of the PL is shown in Fig. 1(b). A customized fluorine-doped fiber and five different types of single-mode fibers are used to construct the fiber bundle. The customized fluorine-doped fiber consists of an inner fluorine-doped layer and an outer pure silica layer. The numerical aperture of the inner fluorine-doped layer is 0.22, which means the refractive index of the inner fluorine-doped layer is much lower than that of SiO_2 . Therefore, at the few-mode end of the PL, radial high-order modes are not allowed. The diameter d_1 of the fluorine-doped layer is 170 μm , and the diameter d_2 of the pure silica layer is 240 μm . The numerical aperture of the

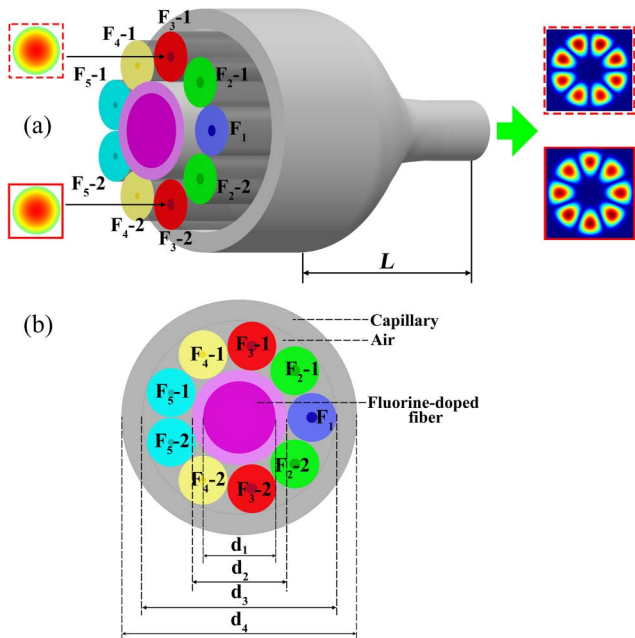


Fig. 1. (a) Schematic of the PL; (b) single-mode end of the PL.

low refractive index capillary is 0.22. The inner diameter d_3 and the outer diameter d_4 of the pretapered low refractive index capillary are 490 and 550 μm , respectively. Fiber F_1 is placed at the right, and the others are symmetrically placed as shown in Fig. 1(b). The same color represents the same fiber. When fundamental mode is injected at the single-mode end of the PL, it will evolve into a corresponding mode at the few-mode end of the PL after passing through the tapered region with length L , as shown in Fig. 1(a). It is worth noting that Fig. 1 is not drawn to scale. The refractive index distributions of five kinds of single-mode fibers are shown in Fig. 2. Except for fiber F_1 , all other single-mode fibers have low refractive index regions around their cores.

Using the finite-element method and based on the experimental data, the geometric modeling of the PL is established, and the effective refractive index (ERI) of the eigenmodes is obtained, as shown in Fig. 3(a). When the fundamental mode is injected at the single-mode end of the PL, the energy will be confined inside the cores of the single-mode fibers when the propagation distance z does not exceed 0.0500 m. There are several crossings in the ERI curves between the propagation distance $z = 0$ and 0.0500 m, as shown in Fig. 3(a). The reason is that there are low doping regions around the core of single-mode fibers F_2 – F_5 , which leads to a faster decrease in the ERI when energy diffuses to the cladding area, resulting in crossing. However, there is no coupling between these modes because they do not overlap spatially when the propagation distance z does not exceed 0.0500 m. As the core size further decreases, the ERI of the mode also further decreases, as shown in Fig. 3(a). Until the fiber core is unable to confine light, energy diffuses to the cladding area. Then, spatial overlap and coupling are possible for modes injected into different cores. When coupling begins, the ERI of LP_{41}^{even} and LP_{41}^{odd} takes the eighth and ninth position. And the intrinsic energy exchanges along the taper between supermodes will make sure that supermodes corresponding to LP_{41}^{even} and LP_{41}^{odd} will always take the eighth and ninth position. The ERI of mode 1 and mode 3 is very close when

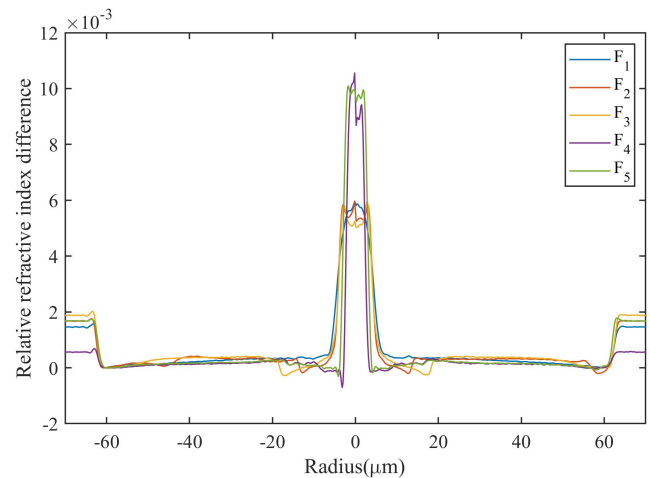


Fig. 2. Refractive index distribution of single-mode fibers.

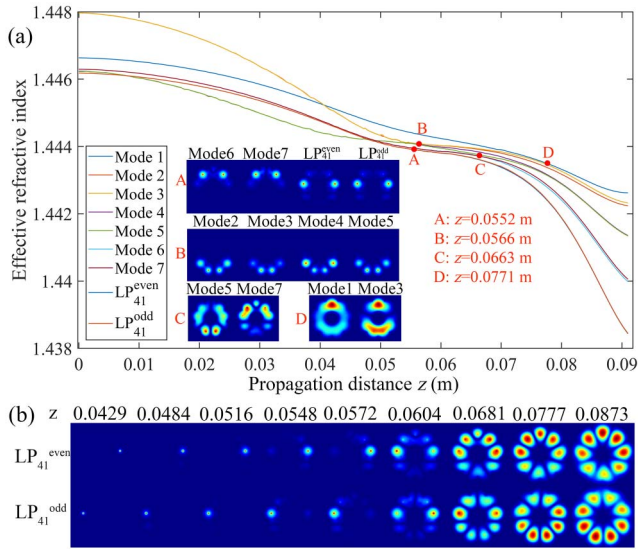


Fig. 3. (a) ERI of eigenmodes along the taper; (b) evolution of LP₄₁^{even} and LP₄₁^{odd}.

the propagation distance $z = 0.0771$ m, and the mode field distributions have a large spatial overlap, as shown by the red mark “D” in Fig. 3(a), which leads to strong coupling between LP₀₁ and LP₁₁ mode groups. The ERI of modes 2–5 is very close when the propagation distance $z = 0.0566$ m, and mode fields of modes 2–5 almost completely overlap in space as shown by the red mark “B” in Fig. 3(a), which leads to strong coupling between LP₁₁ and LP₂₁ mode groups. And when the propagation distance $z = 0.0663$ m, the ERI of mode 5 and mode 7 is close, and a large spatial overlap happens between them, as shown by the red mark “C” in Fig. 3(a), which leads to strong coupling between LP₂₁ and LP₃₁ mode groups. However, when the propagation distance $z = 0.0552$ m, although the ERIs of modes 6, 7 and LP₄₁ mode group are close, the spatial overlap is small as shown by the red mark “A” in Fig. 3(a). Therefore, the coupling between LP₄₁ mode group and modes 6, 7 is weak. In summary, only the LP₄₁ mode group is possible to be excited with high purity. The eigenmodes corresponding to the LP₄₁ mode group at different propagation distances z are shown in Fig. 3(b). It can be seen that LP₄₁^{even} and LP₄₁^{odd} have different evolution paths, which can lead to differences in the purity of excited LP₄₁^{even} and LP₄₁^{odd}.

3. Experiments

The PL is fabricated with a Vytran automated glass processor with an integrated cleaver, using graphite filaments. The diameters of the fluorine-doped capillary and the fluorine-doped fibers are larger than that we need. Therefore, the outer diameter of the fluorine-doped fiber is pretapered to 240 μm. Then the diameter of the fiber bundle will be 490 μm. To facilitate the insertion of the fiber bundle into the capillary, the inner diameter of the low refractive index capillary is pretapered to a size

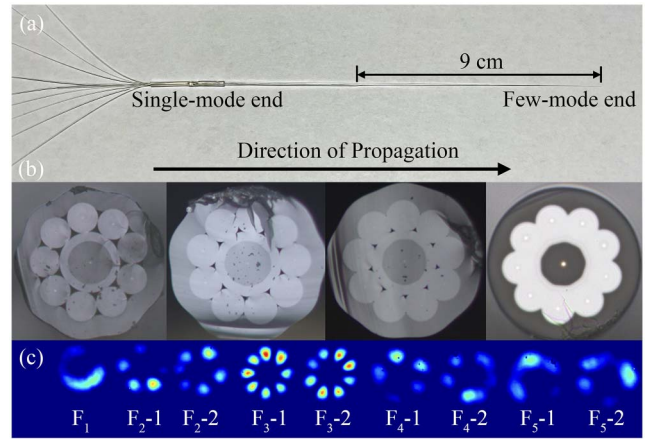


Fig. 4. (a) Image of the fabricated PL; (b) image of the cross section along the taper; (c) output of the PL at 1550 nm with different single-mode fibers as input.

slightly larger than the diameter of the fiber bundle. The coating layer of single-mode fibers will be removed and then combined with the fluorine-doped fiber to form a fiber bundle. With the help of anhydrous ethanol, the fiber bundle can be easily inserted into the capillary. Pretapering with the help of a vacuum pump will be made to further fit the inner wall of the capillary with the fiber bundle. Finally, a final taper with a vacuum pump is made to finish the fabrication of the PL. The online cleaving is finished by the integrated cleaver.

The image of the fabricated PL is shown in Fig. 4(a). The taper length of the PL is close to 9 cm. The diameter of the few-mode end of the fabricated PL is 31 μm, which gives a taper ratio of 0.1047. During the taper process, the air holes at the single-mode end of the PL will gradually collapse until they disappear at the few-mode end, as shown in Fig. 4(b). Then, with different single-mode fibers as input, the mode fields of the output at the few-mode end of the PL are shown in Fig. 4(c). It can be seen that only the output with single-mode fiber F₃ as input has the obvious characteristics of the high-purity LP₄₁ mode group, which is consistent with the discussion about Fig. 3.

4. Results

In order to better analyze the performance of the excitation of the LP₄₁ mode group, tunable lasers (Yenista TUNICS-T100S-HP and Agilent Keysight 8164B) and infrared camera (Xi'an Leading Optoelectronic, LD-SW640171550-UC-G) are used to collect the intensity distributions of LP₄₁^{even} and LP₄₁^{odd}. Due to the lack of a tunable laser at 1360–1460 nm, only the intensity distributions at 1260–1360 nm and 1460–1640 nm are collected. Light from the tunable laser is injected into the single-mode fiber F₃-1/F₃-2 at the single-mode end of the PL, respectively. Then, the fundamental mode in the single-mode fiber evolves into LP₄₁^{even} and LP₄₁^{odd} at the few-mode end of the PL along the taper. The output of the PL is captured by the infrared camera after being collimated by an objective lens.

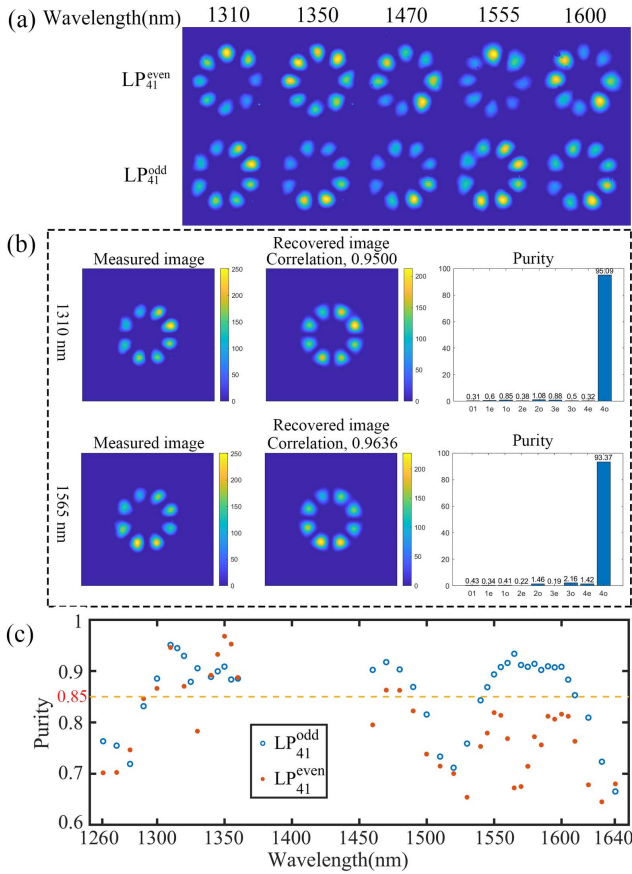


Fig. 5. (a) Intensity distributions of LP_{41}^{even} and LP_{41}^{odd} ; (b) measured image, recovered image, and recovered component of LP_{41}^{odd} at 1310 and 1565 nm; (c) measured purity of LP_{41}^{even} and LP_{41}^{odd} at 1260–1360 nm and 1460–1640 nm.

Intensity distributions of LP_{41}^{even} and LP_{41}^{odd} at several typical wavelengths are shown in Fig. 5(a). It can be seen that in a wide wavelength range, the intensity distributions can maintain the characteristics of eight lobes of LP_{41}^{even} and LP_{41}^{odd} .

Through the numerical mode decomposition method of the collected intensity distribution, the purities of LP_{41}^{even} and LP_{41}^{odd} were measured. The purity of a mode is written as

$$\text{purity}(i) = P_i / \left(\sum P_i \right) \times 100\%, \quad (1)$$

in which P_i is the power of a target mode i at the few-mode end, and $\sum P_i$ is the total power of all modes at the few-mode end.

The mode purity was measured by detecting the mode fields at the output of the PL and executing mode decomposition^[16,17]. First, the intensity distribution was captured by an infrared camera. Second, the real and imaginary parts of the Fourier coefficients from the Fourier expansion were formulated as an equation group. Third, the intensity distribution was reduced to an azimuthal sampling one-dimensional sequence with a certain radius. Finally, we solved the equation group and obtained the amplitudes of each mode component, and then we calculated the mode purity. Based on the recovered mode components, the

intensity image can be reconstructed. Figure 5(b) shows measured image, recovered image, and recovered component of LP_{41}^{odd} at 1310 and 1565 nm. The purity of LP_{41}^{odd} at 1310 and 1565 nm is measured to be about 95.09% and 93.37%, respectively. The correlations between the measured image and the recovered image of LP_{41}^{odd} at 1310 and 1565 nm are 0.9500 and 0.9636, which ensures the credibility and accuracy of the recovered results.

With this method, the purity of LP_{41}^{even} and LP_{41}^{odd} at 1260–1360 nm and 1460–1640 nm is measured, as shown in Fig. 5(c). The highest mode purity of LP_{41}^{odd} in the wavelength range of 1260–1360 nm and 1460–1640 nm is 95.09% at 1310 nm and 93.37% at 1565 nm, respectively, and the highest mode purity of LP_{41}^{even} in the wavelength range of 1260–1360 nm and 1460–1640 nm is 95.26% at 1355 nm and 86.27% at 1470 nm, respectively. The bandwidths of mode purity higher than 85.00% of LP_{41}^{even} and LP_{41}^{odd} are 50 and 155 nm, respectively. The bandwidth of mode purity higher than 85.00% of LP_{41}^{odd} is wider than that of LP_{41}^{even} . This may be because the paths of light injected into single-mode fiber F₃-1/F₃-2 are not exactly the same as shown in Fig. 3(b), which causes differences in the purity of excited LP_{41}^{even} and LP_{41}^{odd} .

The IL of the fabricated PL is also experimentally measured. The IL of an optical device is written as

$$IL = -10 \log_{10}(P_{\text{out}}/P_{\text{in}}), \quad (2)$$

in which P_{in} and P_{out} are the input and output power of the PL, respectively.

The measured ILs of LP_{41}^{even} and LP_{41}^{odd} are shown in Fig. 6. The IL of LP_{41}^{odd} is less than 0.2 dB in the wavelength range of 1260–1360 nm and 1460–1640 nm. And the IL of LP_{41}^{even} is less than 0.4 dB in the wavelength range of 1260–1360 nm and 1460–1640 nm. It can be seen that the ILs of LP_{41}^{even} and LP_{41}^{odd} show obvious differences in the wavelength range of 1460–1640 nm. This is due to gravity and the deviation of the position of the fiber bundle in the temperature field created by the graphite filament; the cross section of the tapered region is not symmetrical during the tapering process. In the short wavelength range, light is better confined. However, in the long wavelength range, the mode field area is larger, making LP_{41}^{even} and LP_{41}^{odd} more sensitive to defects during the manufacturing process. And the evolution

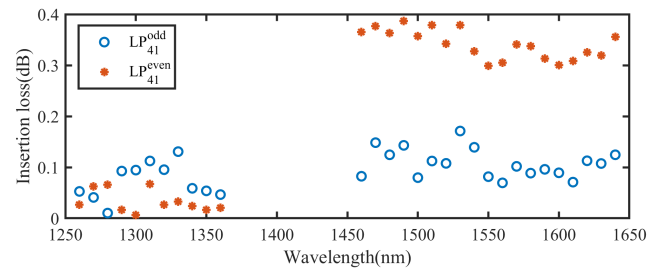


Fig. 6. ILs of LP_{41}^{even} and LP_{41}^{odd} .

paths of LP_{41}^{even} and LP_{41}^{odd} are different, which leads to significant differences in IL within the wavelength range of 1460–1640 nm.

5. Conclusion

In summary, a low-loss, high-purity, and ultrabroadband all-fiber LP_{41} mode converter was proposed and fabricated. Selective excitation of LP_{41}^{even} and LP_{41}^{odd} was realized by tapering a nine-core single-mode fiber bundle with an outer low refractive index capillary. Using tunable laser sources with a limited spectral range, the operating wavelength of the all-fiber LP_{41} mode converter was measured to cover 1260–1360 nm and 1460–1640 nm. By decomposing the collected mode field intensity, the purity of LP_{41}^{odd} at 1310 and 1565 nm was measured to be about 95.09% and 93.37%, respectively. The bandwidths of purity higher than 85.00% of LP_{41}^{even} and LP_{41}^{odd} were 50 and 155 nm, respectively. The IL of LP_{41}^{odd} was less than 0.2 dB at 1260–1360 nm and 1460–1640 nm, and the IL of LP_{41}^{even} was less than 0.4 dB at 1260–1360 nm and 1460–1640 nm. Our work provides a low-loss, high-purity, and ultrabroadband all-fiber LP_{41} mode converter for space-division and wavelength-division multiplexing fiber systems.

Acknowledgement

This work was supported by the National Key Research and Development Program of China (No. 2018YFB1801802) and the National Natural Science Foundation of China (Nos. 61835006 and 62375143).

References

1. W. Chang, M. Feng, B. Mao, P. Wang, Z. Wang, and Y. Liu, "All-fiber fourth-order OAM mode generation employing a long period fiber grating written by preset twist," *J. Lightwave Technol.* **40**, 4804 (2022).
2. S. Mo, H. Zhu, J. Liu, J. Liu, J. Zhang, L. Shen, X. Wang, D. Wang, Z. Li, and S. Yu, "Few-mode optical fiber with a simple double-layer core supporting the O + C + L band weakly coupled mode-division multiplexing transmission," *Opt. Express* **31**, 2467 (2023).
3. A. M. Velázquez-Benítez, K. Y. Guerra-Santillán, R. Caudillo-Viurquez, J. E. Antonio-López, R. Amezcua-Correa, and J. Hernández-Cordero, "Optical trapping and micromanipulation with a photonic lantern-mode multiplexer," *Opt. Lett.* **43**, 1303 (2018).
4. A. V. Newkirk, J. E. Antonio-Lopez, A. Velazquez-Benitez, J. Albert, R. Amezcua-Correa, and A. Schülzgen, "Bending sensor combining multi-core fiber with a mode-selective photonic lantern," *Opt. Lett.* **40**, 5188 (2015).
5. J. Liu, J. Zhang, J. Liu, Z. Lin, Z. Li, Z. Lin, J. Zhang, C. Huang, S. Mo, L. Shen, S. Lin, Y. Chen, R. Gao, L. Zhang, X. Lan, X. Cai, Z. Li, and S. Yu, "1-Pbps orbital angular momentum fibre-optic transmission," *Light: Sci. Appl.* **11**, 202 (2022).
6. J. Fang, J. Li, A. Kong, Y. Xie, C. Lin, Z. Xie, T. Lei, and X. Yuan, "Optical orbital angular momentum multiplexing communication via inversely-designed multiphase plane light conversion," *Photonics Res.* **10**, 2015 (2022).
7. K. H. Lin and W. H. Kuan, "Ultrabroadband long-period fiber gratings for wavelength-tunable doughnut beam generation," *IEEE Photon. Technol. Lett.* **35**, 203 (2023).
8. C. Ma, D. Wang, H. Deng, and L. Yuan, "Stable orbital angular momentum mode generator based on helical long-period fiber grating," *Opt. Fiber Technol.* **73**, 103019 (2022).
9. K. Zhang, P. Wu, J. Dong, D. Du, Z. Yang, C. Xu, H. Guan, H. Lu, W. Qiu, J. Yu, and Z. Chen, "Broadband mode-selective couplers based on tapered side-polished fibers," *Opt. Express* **29**, 19690 (2021).
10. Z. S. Eznaveh, J. C. A. Zacarias, J. E. A. Lopez, K. Shi, G. Milione, Y. Jung, B. C. Thomsen, D. J. Richardson, N. Fontaine, S. G. Leon-Saval, and R. A. Correa, "Photonic lantern broadband orbital angular momentum mode multiplexer," *Opt. Express* **26**, 30042 (2018).
11. M. Feng, W. Chang, B. Mao, H. Guo, Z. Wang, and Y. Liu, "Efficient generation of second-order beam based on angular modulated long-period fiber grating," *Opt. Laser Technol.* **152**, 108131 (2022).
12. W. Chang, M. Feng, P. Wang, Z. Wang, and Y. Liu, "High-efficiency broadband third-order OAM mode converter based on a multi-period preset-twist long-period fiber grating," *Opt. Express* **30**, 47048 (2022).
13. J. Cui, Y. Gao, S. Huang, J. Yu, J. Liu, J. Jia, Y. He, Z. Chen, and J. Li, "Five-LP-mode IM/DD MDM transmission based on degenerate-mode-selective couplers with side-polishing processing," *J. Lightwave Technol.* **41**, 2991 (2023).
14. H. Guo, L. Chen, Z. Shi, W. Chang, L. Gu, Z. Wang, and Y. Liu, "Ultra-low-loss 5-LP mode selective coupler based on fused biconical taper technique," *Opt. Express* **31**, 18050 (2023).
15. A. M. Velázquez-Benítez, J. E. Antonio-López, J. C. Alvarado-Zacarias, N. K. Fontaine, R. Ryf, H. Chen, J. Hernández-Cordero, P. Sillard, C. Okonkwo, S. G. Leon-Saval, and R. Amezcua-Correa, "Scaling photonic lanterns for space-division multiplexing," *Sci. Rep.* **8**, 8897 (2018).
16. B. Mao, Y. Liu, H. Guo, H. Zhang, M. Feng, J. He, Z. Wang, and Z. Li, "An accurate method for measuring the proportions of degenerated spatial modes in fibers," *J. Lightwave Technol.* **38**, 4052 (2020).
17. Z. Shi, B. Mao, Z. Wang, and Y. Liu, "Accurate mode purity measurement of ring core fibers with large mode numbers from the intensity distribution only," *Photonics Res.* **11**, 1592 (2023).